


MARCH 24 2022

Focused beams for high-resolution imaging and other applications **FREE**

Jian-yu Lu 



Proc. Mtgs. Acoust. 45, 020001 (2021)

<https://doi.org/10.1121/2.0001544>



Articles You May Be Interested In

Synthetic aperture imaging for multilayer cylindrical object using an exterior rotating transducer

Rev. Sci. Instrum. (August 2015)

Shape error analysis for reflective nano focusing optics

AIP Conf. Proc. (June 2010)

Energy flux streamlines versus acoustic rays for modeling interaction with rigid boundaries: near field of sound from a circular loudspeaker

Proc. Mtgs. Acoust. (May 2013)



LEARN MORE

Advance your science and career as a member of the
Acoustical Society of America

181st Meeting of the Acoustical Society of America

Seattle, Washington

29 November - 3 December 2021

Biomedical Acoustics: Paper 2aBAb1

Focused beams for high-resolution imaging and other applications

Jian-yu Lu

Department of Bioengineering, The University of Toledo, Toledo, Ohio, 43606; jian-yu.lu@ieee.org

Analytical solutions were obtained for limited diffraction beams such as Bessel beams and X waves, as well as for conventional plane wave, with or without focus in both rectangular and polar coordinates. Using a focused plane wave in transmit and a focused Bessel beam in receive, a high-resolution C-mode image that breaks the diffraction limit of the conventional focused plane wave was obtained using a wave source of 50-mm diameter, 2.5-MHz frequency, 50-mm focal length, and 0.6-mm wavelength for an object at the focus. The two-way (pulse-echo) full-width-at-half-maximum (FWHM) lateral resolution of the image obtained was 0.56 mm. As comparison, the FWHM lateral resolution of the image obtained with the focused plane wave in both transmit and receive was 0.66 mm. The diffraction limit calculated with the FWHM of the square (two-way) of the Jinc function was 0.62 mm. Besides high image resolution, the focused Bessel beam also has a larger depth-of-field and its higher sidelobes were suppressed by the focused plane wave in transmit. In addition, using the analytical solutions developed, an ultrasound image (beam pattern) was produced using a commercial Verasonics 32x32 Matrix Array for visual (retina) stimulation of the brain to help blind people to see objects.

1. INTRODUCTION

Limited-diffraction beams such as Bessel beams¹⁻³ and X waves⁴⁻⁵ have been studied extensively in the past few decades because they have a very large depth of field. For example, these beams have been applied to pulse-echo medical imaging⁶, blood flow velocity vector imaging⁷, nondestructive evaluation (NDE) of materials⁸, tissue characterizations⁹, fast computations of spatial distribution of waves produced by 2D array transducers¹⁰, X-wave transformation¹¹, plane-wave 2D and 3D high-frame rate imaging¹¹⁻¹⁵, and other applications. In addition, because of the spatially invariant properties of the X waves, they have also been studied extensively in Physics¹⁶.

Although limited-diffraction beams have many applications, they have not been studied when they are focused by a lens or using electronic focusing. In this paper, a C-mode image (the imaging plane is perpendicular to the beam axis) was produced using a focused plane wave in transmit and a focused zeroth-order Bessel beam in receive. It is found that the image produced has a high lateral resolution that exceeds the diffraction limit determined by a fixed aperture size and focal length of a planar radiator. Even though limited-diffraction beams are focused, it is found that they still have a larger depth of field as compared to conventional focused beams. In the image, the sidelobes of the Bessel beam were suppressed by the focused plane wave in transmit.

In addition, in this paper, detailed theoretical analyses of both focused and unfocused waves in both rectangular and polar coordinates have been performed. From the theory, an image (beam pattern) was produced for visual (retina) stimulation of the brain to help certain blind people to see an ultrasound version of the optical image¹⁷.

2. THEORETICAL PRELIMINARIES

A. TIME-VARYING WAVES OR PULSES

The isotropic homogenous scalar wave equation is given by (Goodman, Eq. 3-12)¹⁸:

$$\nabla^2 \Phi - \frac{1}{c^2} \frac{\partial^2 \Phi}{\partial t^2} = \frac{\partial^2 \Phi(x_0, y_0, z; t)}{\partial x_0^2} + \frac{\partial^2 \Phi(x_0, y_0, z; t)}{\partial y_0^2} + \frac{\partial^2 \Phi(x_0, y_0, z; t)}{\partial z^2} - \frac{1}{c^2} \frac{\partial^2 \Phi(x_0, y_0, z; t)}{\partial t^2} = 0, \quad (1)$$

where ∇^2 is the Laplace operator, $\Phi(x_0, y_0, z; t)$ is a function representing a spatial and time-varying wave or pulse propagating in an isotropic homogeneous medium and is a solution to the wave equation. (x_0, y_0, z) is a point in the three-dimensional (3D) space, z is the distance that is perpendicular to the wave source (here we assume that the wave source such as ultrasound transducer is on the $x_1 - y_1$ plane), t is the time, and c is the speed of wave in the medium. According to Bracewell (P. 6)¹⁹, the Fourier transform of the wave is given by:

$$\tilde{\Phi}(x_0, y_0, z; \omega) = \mathcal{F}_t \{ \Phi(x_0, y_0, z; t) \} = \int_{-\infty}^{\infty} \Phi(x_0, y_0, z; t) e^{i\omega t} dt, \quad (2)$$

where $\omega = 2\pi f = kc$ is the angular frequency, f is the frequency, $k = \omega/c = 2\pi/\lambda$ is the wave number, λ is the wavelength, \mathcal{F}_t is the Fourier transform in terms of time, $i = \sqrt{-1}$, and the wave field $\tilde{\Phi}(x_0, y_0, z; \omega)$ satisfies the Helmholtz equation (Goodman, Eq. 3-18)¹⁸:

$$(\nabla^2 + k^2) \tilde{\Phi}(x_0, y_0, z; \omega) = 0. \quad (3)$$

Thus, the inverse Fourier transform, \mathcal{F}_ω^{-1} , of the wave field in terms of ω can be used to obtain any time-varying wave or short pulse (Bracewell, P. 6)¹⁹:

$$\Phi(x_0, y_0, z; t) = \mathcal{F}_\omega^{-1} \{ \tilde{\Phi}(x_0, y_0, z; \omega) \} = \frac{1}{2\pi} \int_{-\infty}^{\infty} \tilde{\Phi}(x_0, y_0, z; \omega) e^{-i\omega t} d\omega. \quad (4)$$

B. THE GREEN'S THEOREM

To solve Eq. (3), Green's theorem can be used (Goodman, Eq. 3-14)¹⁸:

$$\iiint_V (\tilde{\Phi} \nabla^2 G - G \nabla^2 \tilde{\Phi}) dV = \iint_S (\tilde{\Phi} \frac{\partial G}{\partial n} - G \frac{\partial \tilde{\Phi}}{\partial n}) ds, \quad (5)$$

where $\tilde{\Phi}$ and G are functions whose first and second partial derivatives are single-valued and continuous within and on the surface S that encloses the volume V , G is a complex-valued Green's function, and $\partial/\partial n$ is a partial derivative in the outward normal direction at each point on S . If G has a discontinued point in V , this point can be excluded by modifying the surface to $S' = S + S_\varepsilon$, where S_ε is a small sphere of radius ε .

Let $G = G(x_0, y_0, z; x_1, y_1) = e^{ikr_{01}}/r_{01}$ be a spherical wave originating from a point (x_0, y_0, z) (Goodman, Eq. 3-15)¹⁸, where r_{01} is the distance between (x_0, y_0, z) and a point (x_1, y_1) on S' . Excluding the discontinuous point (x_0, y_0, z) , Eq. (5) becomes (Goodman, Eq. 3-19)¹⁸:

$$\iint_{S'} (\tilde{\Phi} \frac{\partial G}{\partial n} - G \frac{\partial \tilde{\Phi}}{\partial n}) ds = \iint_S (\tilde{\Phi} \frac{\partial G}{\partial n} - G \frac{\partial \tilde{\Phi}}{\partial n}) ds + \iint_{S_\varepsilon} (\tilde{\Phi} \frac{\partial G}{\partial n} - G \frac{\partial \tilde{\Phi}}{\partial n}) ds \equiv 0, \quad (6)$$

i.e.,

$$-\iint_{S_\varepsilon} (\tilde{\Phi} \frac{\partial G}{\partial n} - G \frac{\partial \tilde{\Phi}}{\partial n}) ds = \iint_S (\tilde{\Phi} \frac{\partial G}{\partial n} - G \frac{\partial \tilde{\Phi}}{\partial n}) ds. \quad (7)$$

Eq. (6) is true because both $\tilde{\Phi}$ and G satisfy the Helmholtz equation in Eq. (3) on S' . Since $\tilde{\Phi}$ is continuous everywhere on S and at (x_0, y_0, z) , as $\varepsilon \rightarrow 0$ the left-hand-side of Eq. (7) becomes (Goodman, Eq. 3-21)¹⁸:

$$\begin{aligned} -\lim_{\varepsilon \rightarrow 0} \iint_{S_\varepsilon} (\tilde{\Phi} \frac{\partial G}{\partial n} - G \frac{\partial \tilde{\Phi}}{\partial n}) ds &= -\lim_{\varepsilon \rightarrow 0} \iint_{S_\varepsilon} (\tilde{\Phi} \frac{\partial G}{\partial r_{01}} \cos(\widehat{\vec{n}, \vec{r}_{01}}) - G \frac{\partial \tilde{\Phi}}{\partial n}) ds = -\lim_{\varepsilon \rightarrow 0} \iint_{S_\varepsilon} (\tilde{\Phi} \frac{\partial G}{\partial \varepsilon} \cos(\widehat{\vec{n}, \vec{\varepsilon}}) - (\frac{e^{ik\varepsilon}}{\varepsilon}) \frac{\partial \tilde{\Phi}}{\partial n}) ds \\ &= -\lim_{\varepsilon \rightarrow 0} (4\pi\varepsilon^2) \{ \tilde{\Phi} [(ik - \frac{1}{\varepsilon}) \frac{e^{ik\varepsilon}}{\varepsilon} \cos(\widehat{\vec{n}, \vec{\varepsilon}})] - (\frac{e^{ik\varepsilon}}{\varepsilon}) \frac{\partial \tilde{\Phi}}{\partial n} \} = -4\pi \tilde{\Phi}(x_0, y_0, z; \omega) \end{aligned} \quad (8)$$

where $r_{01} = \varepsilon$ on S_ε with surface area $4\pi\varepsilon^2$, $\cos(\widehat{\vec{n}, \vec{\varepsilon}}) = -1$ is a cosine of the angle between the two vectors \vec{n} and $\vec{\varepsilon}$. Inserting Eq. (8) into Eq. (7), one obtains the integral theorem of Helmholtz and Kirchhoff (Goodman, Eq. 3-21)¹⁸:

$$\tilde{\Phi}(x_0, y_0, z; \omega) = \frac{1}{4\pi} \iint_S (G \frac{\partial \tilde{\Phi}}{\partial n} - \tilde{\Phi} \frac{\partial G}{\partial n}) ds. \quad (9)$$

The surface area S in Eq. (9) can be reduced to a planar area Σ , where the wave source (such as a transducer) is located, under the assumption of the Sommerfeld radiation condition (Goodman, Eq. 3-22)¹⁸ and the two Kirchhoff's assumptions (the assumptions or the Kirchhoff's boundary conditions are valid when $\Sigma \gg \lambda$) (Goodman, P. 44)¹⁸, i.e., (Goodman, Eq. 3-24)¹⁸:

$$\tilde{\Phi}(x_0, y_0, z; \omega) = \frac{1}{4\pi} \iint_\Sigma (G \frac{\partial \tilde{\Phi}}{\partial n} - \tilde{\Phi} \frac{\partial G}{\partial n}) ds. \quad (10)$$

C. RAYLEIGH-SOMMERFELD SOLUTIONS FOR SINGLE-FREQUENCY WAVE FIELD

The two Kirchhoff boundary conditions above are inconsistent with the potential field theory (Goodman, P. 46)¹⁸. This inconsistency can be removed by choosing the following Green's function since it does not need to assume that both $\tilde{\Phi}$ and its normal derivative are zero in the planar area outside Σ (Goodman, Eq. 3-31)¹⁸:

$$G_- = G_-(x_0, y_0, z; x_1, y_1) = \frac{e^{ikr_{01}}}{r_{01}} - \frac{e^{ik\tilde{r}_{01}}}{\tilde{r}_{01}} \equiv 0 \quad (\text{on } \Sigma), \quad \text{or} \quad G_+ = G_+(x_0, y_0, z; x_1, y_1) = \frac{e^{ikr_{01}}}{r_{01}} + \frac{e^{ik\tilde{r}_{01}}}{\tilde{r}_{01}}, \quad (11)$$

where r_{01} and \tilde{r}_{01} are the distances from a point at (x_0, y_0, z) to a point (x_1, y_1) on Σ and from the mirror point $(\tilde{x}_0, \tilde{y}_0, -z)$ of (x_0, y_0, z) to (x_1, y_1) (i.e., the two points are mirroring in terms of the $x_1 - y_1$ plane). The normal derivatives of G_- and G_+ above are given by (Goodman, Eq. 3-33)¹⁸:

$$\begin{aligned} \frac{\partial G_-}{\partial n} &= (ik - \frac{1}{r_{01}}) \frac{e^{ikr_{01}}}{r_{01}} [\cos(\widehat{\vec{n}, \vec{r}_{01}}) - \cos(\widehat{\vec{n}, \tilde{\vec{r}}_{01}})] = 2(ik - \frac{1}{r_{01}}) \frac{e^{ikr_{01}}}{r_{01}} \frac{z}{r_{01}}, \\ \text{and } \frac{\partial G_+}{\partial n} &= (ik - \frac{1}{r_{01}}) \frac{e^{ikr_{01}}}{r_{01}} [\cos(\widehat{\vec{n}, \vec{r}_{01}}) + \cos(\widehat{\vec{n}, \tilde{\vec{r}}_{01}})] \equiv 0 \quad (\text{on } \Sigma), \end{aligned} \quad (12)$$

where $\cos(\widehat{\vec{n}, \vec{r}_{01}}) = -\cos(\widehat{\vec{n}, \tilde{\vec{r}}_{01}}) = z/r_{01}$ is the cosine of the angles between the two vectors \vec{n} and \vec{r}_{01} , and vectors \vec{n} and $\tilde{\vec{r}}_{01}$ (both \vec{r}_{01} and $\tilde{\vec{r}}_{01}$ are pointing towards the point (x_1, y_1) on Σ); and \vec{n} is the vector that is normal to Σ and is outward pointing from the wave volume (x_0, y_0, z) . Using $G_- \equiv 0$ (Eq. (11)) and $\partial G_+ / \partial n \equiv 0$ (Eq. (12)), Eq. (9) can be simplified to the first and the second Rayleigh-Sommerfeld solutions:

$$\tilde{\Phi}(x_0, y_0, z; \omega) = -\frac{1}{4\pi} \int_{-\infty}^{\infty} \int_{-\infty}^{\infty} \tilde{\Phi} \frac{\partial G_-}{\partial n} dx_1 dy_1, \text{ and } \tilde{\Phi}(x_0, y_0, z; \omega) = \frac{1}{4\pi} \int_{-\infty}^{\infty} \int_{-\infty}^{\infty} G_+ \frac{\partial \tilde{\Phi}}{\partial n} dx_1 dy_1, \text{ respectively} \quad (13)$$

Unlike Eq. (10), the first and second Rayleigh-Sommerfeld solutions in Eq. (13) only need to know either $\tilde{\Phi}$ or $\partial \tilde{\Phi} / \partial n$. In fact, Eq. (10) is an arithmetic average of the two solutions in Eq. (13) (Goodman, Eq. 3-50)¹⁸.

Using $\partial G_- / \partial n$ in Eq. (12), from the first Rayleigh-Sommerfeld solution in Eq. (13), the Rayleigh-Sommerfeld diffraction formula is obtained (for simplicity, in the remaining of the paper the first Rayleigh-Sommerfeld solution in Eq. (13) will be used, also, $\tilde{\Phi}_1 = \tilde{\Phi}_1(x_1, y_1; \omega)$ is used to represent wave field at the source plane $\tilde{\Phi}(x_1, y_1, z=0; \omega)$) (Goodman, Eq. 3-41)¹⁸:

$$\tilde{\Phi}(x_0, y_0, z; \omega) = -\frac{1}{4\pi} \int_{-\infty}^{\infty} \int_{-\infty}^{\infty} [2(ik - \frac{1}{r_{01}}) \frac{e^{ikr_{01}}}{r_{01}} \frac{z}{r_{01}}] \tilde{\Phi}_1 dx_1 dy_1 = \frac{z}{i\lambda} \int_{-\infty}^{\infty} \int_{-\infty}^{\infty} (1 + \frac{i\lambda}{2\pi r_{01}}) \tilde{\Phi}_1(x_1, y_1; \omega) \frac{e^{ikr_{01}}}{r_{01}^2} dx_1 dy_1. \quad (14)$$

D. FRESNEL APPROXIMATION

I. IN RECTANGULAR COORDINATES

Eq. (14) can be simplified if $(x_0 - x_1)^2 + (y_0 - y_1)^2 \ll z^2$ and the r_{01} approximation below can be used in the exponential term and $r_{01} \approx z$ can be used in the denominators of Eq. (14) (Goodman, Eq. 4-13)¹⁸:

$$r_{01} = z \sqrt{1 + (\frac{x_0 - x_1}{z})^2 + (\frac{y_0 - y_1}{z})^2} \approx z [1 + \frac{1}{2} (\frac{x_0 - x_1}{z})^2 + \frac{1}{2} (\frac{y_0 - y_1}{z})^2] = z + \frac{1}{2z} [(x_0 - x_1)^2 + (y_0 - y_1)^2]. \quad (15)$$

Eq. (14) thus simplified is called the Fresnel diffraction integral (or the Fresnel approximation of the Rayleigh-Sommerfeld diffraction formula) and is given by the following Fourier transform (Goodman, Eq. 4-17)¹⁸:

$$\begin{aligned} \tilde{\Phi}(x_0, y_0, z; \omega) &= \frac{e^{ikz}}{i\lambda z} (1 + \frac{i\lambda}{2\pi z}) e^{i\frac{k}{2z}(x_0^2 + y_0^2)} \int_{-\infty}^{\infty} \int_{-\infty}^{\infty} [\tilde{\Phi}_1(x_1, y_1; \omega) e^{i\frac{k}{2z}(x_1^2 + y_1^2)}] e^{-i[(\frac{kx_0}{z})x_1 + (\frac{ky_0}{z})y_1]} dx_1 dy_1 \\ &= \frac{e^{ikz}}{i\lambda z} (1 + \frac{i\lambda}{2\pi z}) e^{i\frac{k}{2z}(x_0^2 + y_0^2)} \mathcal{F}_{x_1, y_1} \{ \tilde{\Phi}_1(x_1, y_1; \omega) e^{i\frac{k}{2z}(x_1^2 + y_1^2)} \} (k_{x_0}, k_{y_0}) \end{aligned} \quad (16)$$

where \mathcal{F}_{x_1, y_1} is the Fourier transform in terms of x_1 and y_1 , and k_{x_0} and k_{y_0} are given by:

$$k_{x_0} = k \frac{x_0}{z} = k \frac{r_0}{z} \cos \phi = k_0 \cos \phi; \quad k_{y_0} = k \frac{y_0}{z} = k \frac{r_0}{z} \sin \phi = k_0 \sin \phi; \quad k_0 = \sqrt{k_{x_0}^2 + k_{y_0}^2} = k \frac{r_0}{z}; \quad r_0 = \sqrt{x_0^2 + y_0^2}, \quad (17)$$

where k_0 and ϕ are variables in the polar coordinates in the Fourier domain. Eq. (16) is generally valid as long as the integral is dominated by values at $x_1 \approx x_0$ and $y_1 \approx y_0$, even Eq. (15) is not necessarily satisfied. If

z is very large so that the so called “antenna designer’s formula” $z > 2D^2/\lambda$ is satisfied, where D is the diameter of Σ , Eq. (16) can be further simplified as the Fraunhofer approximation (Goodman, Eq. 4-25)¹⁸.

II. IN POLAR COORDINATES

Using polar coordinates $r_1 - \theta$ in the $x_1 - y_1$ plane where the wave source is located, where $x_1 = r_1 \cos \theta$, $y_1 = r_1 \sin \theta$, and $r_1 = \sqrt{x_1^2 + y_1^2}$, the terms in the integration in Eq. (16) can be written as

$$\tilde{\Phi}_1(x_1, y_1; \omega) e^{\frac{ik}{2z}(x_1^2 + y_1^2)} = \tilde{\Phi}_1(r_1, \theta; \omega) e^{\frac{ik}{2z}r_1^2} \quad \text{and} \quad e^{-i[(\frac{x_0}{z})x_1 + (\frac{y_0}{z})y_1]} = e^{-ik_0 r_1 (\cos \phi \cos \theta + \sin \phi \sin \theta)} = e^{-ik_0 r_1 \cos(\theta - \phi)}. \quad (18)$$

Inserting Eq. (18) into Eq. (16) and transforming from rectangular to polar coordinates, we have:

$$\tilde{\Phi}(x_0, y_0, z; \omega) = \frac{e^{ikz}}{i\lambda z} \left(1 + \frac{i\lambda}{2\pi z}\right) e^{\frac{ik}{2z}r_0^2} \int_{-\pi}^{\pi} \int_0^{\infty} [\tilde{\Phi}_1(r_1, \theta; \omega) e^{\frac{ik}{2z}r_1^2}] e^{-ik_0 r_1 \cos(\theta - \phi)} r_1 dr_1 d\theta. \quad (19)$$

Since the second equation in Eq. (18) has the following identity (Morse & Feshbach, P.620)²⁰:

$$e^{-ik_0 r_1 \cos(\theta - \phi)} = e^{(-i)k_0 r_1 \cos(\theta - \phi)} = \sum_{n=-\infty}^{\infty} (-i)^n J_n(k_0 r_1) e^{(-i)n(\theta - \phi)} = \sum_{n=-\infty}^{\infty} i^{-n} J_n(k_0 r_1) e^{-in(\theta - \phi)}, \quad (20)$$

and the wave source in the square brackets of Eq. (19) is always periodic (2π period) in terms of θ and thus it can be represented as a Fourier series pair (Baddour, Eqs. (14) and (15); Cornacchio & Soni, Eq. (5))²¹⁻²²:

$$\tilde{\Phi}_1(r_1, \theta; \omega) e^{\frac{ik}{2z}r_1^2} = e^{\frac{ik}{2z}r_1^2} \sum_{n=-\infty}^{\infty} \tilde{\Phi}_{1n}(r_1; \omega) e^{in\theta}, \quad \text{with coefficients:} \quad \tilde{\Phi}_{1n}(r_1; \omega) = \frac{1}{2\pi} \int_0^{2\pi} \tilde{\Phi}_1(r_1, \theta; \omega) e^{-in\theta} d\theta, \quad (21)$$

Eq. (19) can be represented with an n th-order Hankel transform $\mathfrak{H}_n\{\}$ as follows (Baddour, Eqs. (1), (18), and (19); Cornacchio & Soni, Eqs. (6) and (7))²¹⁻²²:

$$\begin{aligned} \tilde{\Phi}(x_0, y_0, z; \omega) &= \frac{e^{ikz}}{i\lambda z} \left(1 + \frac{i\lambda}{2\pi z}\right) e^{\frac{ik}{2z}r_0^2} \int_{-\pi}^{\pi} \int_0^{\infty} [e^{\frac{ik}{2z}r_1^2} \sum_{m=-\infty}^{\infty} \tilde{\Phi}_{1m}(r_1; \omega) e^{im\theta}] [\sum_{n=-\infty}^{\infty} i^{-n} J_n(k_0 r_1) e^{-in(\theta - \phi)}] r_1 dr_1 d\theta \\ &= \frac{e^{ikz}}{i\lambda z} \left(1 + \frac{i\lambda}{2\pi z}\right) e^{\frac{ik}{2z}r_0^2} \sum_{m=-\infty}^{\infty} \sum_{n=-\infty}^{\infty} \left\{ \int_0^{\infty} e^{\frac{ik}{2z}r_1^2} \tilde{\Phi}_{1m}(r_1; \omega) i^{-n} J_n(k_0 r_1) r_1 dr_1 \right\} \left[e^{in\phi} \begin{cases} 2\pi, & m = n \\ 0, & \text{Otherwise} \end{cases} \right] \\ &= \frac{e^{ikz}}{i\lambda z} \left(1 + \frac{i\lambda}{2\pi z}\right) e^{\frac{ik}{2z}r_0^2} \sum_{n=-\infty}^{\infty} 2\pi i^{-n} e^{in\phi} \mathfrak{H}_n \{ e^{\frac{ik}{2z}r_1^2} \tilde{\Phi}_{1n}(r_1; \omega) \} (k_0), \quad \text{where} \quad \mathfrak{H}_n \{ \} = \int_0^{\infty} [e^{\frac{ik}{2z}r_1^2} \tilde{\Phi}_{1n}(r_1; \omega)] J_n(k_0 r_1) r_1 dr_1 \end{aligned} \quad (22)$$

Using the integration relationship of $\tilde{\Phi}_{1n}(r_1; \omega)$ in Eq. (21), Eq. (22) can be expressed in terms of $\tilde{\Phi}_1$:

$$\tilde{\Phi}(x_0, y_0, z; \omega) = \frac{e^{ikz}}{i\lambda z} \left(1 + \frac{i\lambda}{2\pi z}\right) e^{\frac{ik}{2z}r_0^2} \sum_{n=-\infty}^{\infty} i^{-n} e^{in\phi} \mathfrak{H}_n \left\{ e^{\frac{ik}{2z}r_1^2} \int_0^{2\pi} \tilde{\Phi}_1(r_1, \theta; \omega) e^{-in\theta} d\theta \right\} (k_0). \quad (23)$$

E. SPECIAL CASES FOR CIRCULAR UNFOCUSED WAVE SOURCES UNDER FRESNEL APPROXIMATION

I. SEPARABLE-VARIABLE WAVE SOURCES

If the variables of the wave source functions are separable between r_1 and θ , i.e., $\tilde{\Phi}_1(r_1, \theta; \omega) = \tilde{\Phi}_{1r_1}(r_1; \omega) \tilde{\Phi}_{1\theta}(\theta; \omega)$, Eq. (23) can be simplified to (Goodman, Eq. 2-22)¹⁸:

$$\tilde{\Phi}(x_0, y_0, z; \omega) = \frac{e^{ikz}}{i\lambda z} \left(1 + \frac{i\lambda}{2\pi z}\right) e^{\frac{ik}{2z}r_0^2} \sum_{n=-\infty}^{\infty} i^{-n} e^{in\phi} \int_0^{2\pi} \tilde{\Phi}_{1\theta}(\theta; \omega) e^{-in\theta} d\theta \mathfrak{H}_n \{ e^{\frac{ik}{2z}r_1^2} \tilde{\Phi}_{1r_1}(r_1; \omega) \} (k_0). \quad (24)$$

II. NTH-ORDER BESSEL BEAMS

If in Eq. (24) the wave source is an n th-order Bessel weighting function $\tilde{\Phi}_1(r_1, \theta; \omega) = J_n(\alpha r_1) e^{in\theta}$, where n is an integer and α is a scaling factor of the Bessel function, a Bessel beam can be produced^{1,3}:

$$\begin{aligned} \tilde{\Phi}_{B_n}(x_0, y_0, z; \omega) &= \frac{e^{ikz}}{i\lambda z} \left(1 + \frac{i\lambda}{2\pi z}\right) e^{\frac{k}{2z} r_0^2} \sum_{m=-\infty}^{\infty} i^{-m} e^{im\phi} \left[\begin{cases} 2\pi, & m = n \\ 0, & \text{Otherwise} \end{cases} \right] \mathcal{J}_m \left\{ e^{\frac{k}{2z} r_1^2} J_n(\alpha r_1) \right\} (k_0) \\ &= \frac{e^{ikz}}{i\lambda z} \left(1 + \frac{i\lambda}{2\pi z}\right) e^{\frac{k}{2z} r_0^2} (2\pi i^{-n} e^{in\phi}) \mathcal{J}_n \left\{ e^{\frac{k}{2z} r_1^2} J_n(\alpha r_1) \right\} (k_0), \quad \text{where} \quad \int_0^{2\pi} e^{i(n-m)\theta} d\theta = \begin{cases} 2\pi, & m = n \\ 0, & \text{Otherwise} \end{cases}. \end{aligned} \quad (25)$$

III. NTH-ORDER X-WAVES

Also from Eq. (24), if the wave source is an n th-order X-wave weighting function $\tilde{\Phi}_1(r_1, \theta; \omega) = J_n(kr_1 \sin \varsigma) e^{in\theta}$, where n is an integer and ς is the Axicon angle²³, an X wave can be produced^{4,5}:

$$\begin{aligned} \tilde{\Phi}_{X_n}(x_0, y_0, z; \omega) &= \frac{e^{ikz}}{i\lambda z} \left(1 + \frac{i\lambda}{2\pi z}\right) e^{\frac{k}{2z} r_0^2} \sum_{m=-\infty}^{\infty} i^{-m} e^{im\phi} \left[\begin{cases} 2\pi, & m = n \\ 0, & \text{Otherwise} \end{cases} \right] \mathcal{J}_m \left\{ e^{\frac{k}{2z} r_1^2} J_n(kr_1 \sin \varsigma) \right\} (k_0) \\ &= \frac{e^{ikz}}{i\lambda z} \left(1 + \frac{i\lambda}{2\pi z}\right) e^{\frac{k}{2z} r_0^2} (2\pi i^{-n} e^{in\phi}) \mathcal{J}_n \left\{ e^{\frac{k}{2z} r_1^2} J_n(kr_1 \sin \varsigma) \right\} (k_0), \quad \text{where} \quad \int_0^{2\pi} e^{i(n-m)\theta} d\theta = \begin{cases} 2\pi, & m = n \\ 0, & \text{Otherwise} \end{cases}. \end{aligned} \quad (26)$$

IV. PLANE WAVE

A plane wave can be obtained using Eq. (24) if the wave source function is a constant, say, $\tilde{\Phi}_1(r_1, \theta; \omega) = 1$ (i.e., setting $n = 0$ and $\alpha = 0$ in Eq. (25) or setting $\varsigma = 0$ in Eq. (26)) and when the Fresnel approximation holds:

$$\tilde{\Phi}_p(x_0, y_0, z; \omega) = \frac{e^{ikz}}{i\lambda z} \left(1 + \frac{i\lambda}{2\pi z}\right) e^{\frac{k}{2z} r_0^2} (2\pi) \mathcal{J}_0 \left\{ e^{\frac{k}{2z} r_1^2} \right\} (k_0). \quad (27)$$

F. SPECIAL CASES FOR FOCUSED WAVE SOURCES UNDER FRESNEL APPROXIMATION

I. FOCUSED WAVES IN RECTANGULAR COORDINATES

Under the Fresnel approximation, to focus the waves produced by the wave source $\tilde{\Phi}_1(x_1, y_1; \omega)$ located on the $x_1 - y_1$ plane (see Eq. (16)), a thin lens can be attached immediately behind the wave source or an electronic focusing can be implemented with an array transducer to introduce spatial phase shifts. With the paraxial approximation (i.e., considering the wave field near the axis of the lens), the spherical surface of the lens can be approximated with a parabolic phase surface. In this case, the phase shift introduced by the lens is given by $\exp\{-i[k/(2F)](x_1^2 + y_1^2)\} = \exp\{-i[k/(2F)]r_1^2\}$ (Goodman, Eq. 5-10)¹⁸, where F is the focal length of the lens or electronic focusing. Expressing the wave source in Eq. (16) to include the phase shifts, i.e., $\tilde{\Phi}_1(x_1, y_1; \omega) = \tilde{\Phi}'_1(x_1, y_1; \omega) \exp\{-i[k/(2F)](x_1^2 + y_1^2)\}$ at the $x_1 - y_1$ plane, where $\tilde{\Phi}'_1(x_1, y_1; \omega)$ is a modified wave source that does not include the phase shifts, a focused beam at distance $z = F$ can be produced via a direct Fourier transform $\mathcal{F}_{x_1, y_1} \{ \}$ of the modified wave sources $\tilde{\Phi}'_1(x_1, y_1; \omega)$ (Goodman, Eq. 5-14)¹⁸:

$$\tilde{\Phi}(x_0, y_0, z = F; \omega) = \frac{e^{ikF}}{i\lambda F} \left(1 + \frac{i\lambda}{2\pi F}\right) e^{\frac{k}{2F}(x_0^2 + y_0^2)} \mathcal{F}_{x_1, y_1} \{ \tilde{\Phi}'_1(x_1, y_1; \omega) \} (k_{x_0}, k_{y_0}), \quad (28)$$

where $k_{x_0} = kx_0 / F$ and $k_{y_0} = ky_0 / F$ are given by Eq. (17). If the wave source has a dimension $D \times D$, the integration limits in the Fourier transform will be from $-a$ to a , where $D = 2a$.

II. FOCUSED WAVE IN POLAR COORDINATES

a. An Arbitrary Focused Waves:

Also under the Fresnel approximation, in polar coordinates, after including the focusing phase shifts (either by a lens or electronic focusing) to the wave source, the wave source in Eq. (23) at the $x_1 - y_1$ plane can be expressed as $\tilde{\Phi}_1(r_1, \theta; \omega) = \tilde{\Phi}'_1(r_1, \theta; \omega) \exp\{-i[k/(2F)]r_1^2\}$, where $\tilde{\Phi}'_1(r_1, \theta; \omega)$ is a modified wave source that does not include the phase shifts. At the axial distance $z = F$ (focal distance), Eq. (23) can be simplified since the phase term ($\exp\{i[k/(2F)]r_1^2\}$) in the Hankel transform is removed (Goodman, Eq. 5-14)¹⁸:

$$\tilde{\Phi}(x_0, y_0, z = F; \omega) = \frac{e^{ikF}}{i\lambda F} \left(1 + \frac{i\lambda}{2\pi F}\right) e^{i\frac{k}{2F}r_0^2} \sum_{n=-\infty}^{\infty} i^{-n} e^{in\phi} \mathfrak{H}_n \left\{ \int_0^{2\pi} \tilde{\Phi}'_1(r_1, \theta; \omega) e^{-in\theta} d\theta \right\} (k_0). \quad (29)$$

If the variables of the wave source function are separable, i.e., $\tilde{\Phi}'_1(r_1, \theta; \omega) = \tilde{\Phi}'_{1r_1}(r_1; \omega) \tilde{\Phi}'_{1\theta}(\theta; \omega)$, Eq. (29) becomes (if the wave source has a diameter of $D = 2a$, where a is the radius, the integration limits in the Hankel transform will be from 0 to a):

$$\tilde{\Phi}(x_0, y_0, z = F; \omega) = \frac{e^{ikF}}{i\lambda F} \left(1 + \frac{i\lambda}{2\pi F}\right) e^{i\frac{k}{2F}r_0^2} \sum_{n=-\infty}^{\infty} i^{-n} e^{in\phi} \int_0^{2\pi} \tilde{\Phi}'_{1\theta}(\theta; \omega) e^{-in\theta} d\theta \mathfrak{H}_n \{ \tilde{\Phi}'_{1r_1}(r_1; \omega) \} (k_0). \quad (30)$$

b. Focused n th-order Bessel beams:

If the n th-order Bessel beam in Eq. (25) is focused, as shown in Eqs. (29) and (30), the phase term in the Hankel transform can be removed. Thus, at the focal distance $z = F$, a closed form of Eq. (25) can be obtained (Morse & Feshbach, P.943; Gradshteyn & Ryzhik, P. 661)^{20,24}:

$$\tilde{\Phi}_{B_n}(x_0, y_0, z = F; \omega) = \frac{e^{ikF}}{i\lambda F} \left(1 + \frac{i\lambda}{2\pi F}\right) e^{i\frac{k}{2F}r_0^2} (2\pi i^{-n} e^{in\phi}) \mathfrak{H}_n \{ J_n(\alpha r_1) \} (k_0), \quad (31)$$

where $\mathfrak{H}_n \{ \} = \int_0^a J_n(\alpha r_1) J_n(k_0 r_1) r_1 dr_1 = \frac{\delta(\alpha - k_0)}{\sqrt{ak_0}}$,

where $\delta(a - k_0)$ a shifted Dirac-Delta function and the shift amount is given by $k_0 = k(r_0 / F) = \alpha$ or by the radial distance $r_0 = (F / k)\alpha$. If the diameter of the wave source is $D = 2a$, the Hankel transform in Eq. (31) is given by another closed form (Morse & Feshbach, P.619; Gradshteyn & Ryzhik, P.664)^{20,24}:

$$\begin{aligned} \mathfrak{H}_n \{ \} &= \int_0^a J_n(\alpha r_1) J_n(k_0 r_1) r_1 dr_1 = \frac{a[k_0 J_n(\alpha a) J'_n(k_0 a) - \alpha J_n(k_0 a) J'_n(\alpha a)]}{\alpha^2 - k_0^2} \\ &= \frac{a[\alpha J_n(k_0 a) J_{n+1}(\alpha a) - k_0 J_n(\alpha a) J_{n+1}(k_0 a)]}{\alpha^2 - k_0^2}, \quad \text{where } J'_n(x) = \frac{n}{x} J_n(x) - J_{n+1}(x) \end{aligned} \quad (32)$$

This shows that the field at the focus of a Bessel beam is a width modulated ring. The width of the ring will decrease to 0 as the radius becomes infinity. Thus, the truncation of the transducer aperture to D leads to a sharp peak at the center of the ring, which is used for high resolution imaging in this study. Notice that the closed-form solutions in Eqs. (31) and (32) are valid only when $r_0 \ll a$ and thus their predictions of the positions of the rings are only an approximation.

c. Focused n th-order X waves:

For an n th-order X wave focused at distance F , the wave field at $z = F$ is the same as that given in Eq. (31) except that α is replaced with $k \sin \zeta$:

$$\tilde{\Phi}_{X_n}(x_0, y_0, z = F; \omega) = \frac{e^{ikF}}{i\lambda F} \left(1 + \frac{i\lambda}{2\pi F}\right) e^{i\frac{k}{2F}r_0^2} (2\pi i^{-n} e^{in\phi}) \mathfrak{J}_n \{J_n(kr_1 \sin \zeta)\} (k_0). \quad (33)$$

If the wave source is of diameter $D = 2a$, the X wave at the focus is given by Eqs. (32) and (33) with $\alpha = k \sin \zeta$. From Eqs. (31) and (33), it is clear that unlike focused Bessel beams, the ring position of X wave is independent of k and is determined only by F and ζ .

d. Focused plane wave and lateral image resolution:

The focused plane wave produced by a wave source of diameter D and focal length F is a special case of the Bessel beams or X waves when either $\alpha = 0$ or $\zeta = 0$ in Eq. (31) or (33) (Goodman, Eq. 4-30)¹⁸:

$$\tilde{\Phi}_p(x_0, y_0, z = F; \omega) = \frac{e^{ikF}}{i\lambda F} \left(1 + \frac{i\lambda}{2\pi F}\right) e^{i\frac{k}{2F}r_0^2} (2\pi) \mathfrak{J}_0 \left\{ \text{circ}\left(\frac{r_1}{a}\right) \right\} (k_0), \quad \text{where} \quad \text{circ}\left(\frac{r_1}{a}\right) = \begin{cases} 1, & r_1 < a \\ 1/2, & r_1 = a \\ 0, & \text{Otherwise} \end{cases}. \quad (34)$$

Setting $\alpha = 0$ and $n = 0$ in Eq. (32) and using Eq. (31), a closed form solution of Eq. (34) can be obtained (Goodman, Eqs. 2-35 and 4-31)¹⁸:

$$\tilde{\Phi}_p(x_0, y_0, z = F; \omega) = \frac{e^{ikF}}{i\lambda F} \left(1 + \frac{i\lambda}{2\pi F}\right) e^{i\frac{k}{2F}r_0^2} (2\pi) \frac{a[-k_0 J_1(k_0 a)]}{-k_0^2} = \frac{e^{ikF}}{i\lambda F} \left(1 + \frac{i\lambda}{2\pi F}\right) e^{i\frac{k}{2F}r_0^2} [\pi a^2 \text{Jinc}(k_0 a)], \quad (35)$$

where

$$\text{Jinc}(k_0 a) = \frac{2J_1(k_0 a)}{k_0 a} = \frac{2J_1[(kr_0 / F)a]}{(kr_0 / F)a} = \frac{2J_1[(ka / F)r_0]}{(ka / F)r_0}, \quad (36)$$

is the Jinc function that produces the Airy pattern (Goodman, Eq. 2-35)¹⁸. Because $\text{Jinc}(3.8317) = 0$, according to the Rayleigh criterion we obtain the lateral resolution PR_{Airy} of the focused plane wave:

$$PR_{\text{Airy}} = r_0 = 3.8317 \frac{F}{ka} = [2 \times 3.8317 / (2\pi)] \times \lambda \frac{F}{D} \approx 1.22 \lambda F / D. \quad (37)$$

The lateral resolution of an imaging system can also be measured with the full width at half maximum (FWHM) of the Jinc function in Eq. (36), which gives $PR_{\text{FWHM}} = 2r_0 \approx 1.41 \lambda F / D$ since $\text{Jinc}(2.2151) = 0.5$. If $F = 50$ mm, $D = 50$ mm, $f = 2.5$ MHz, and $c = 1500$ m/s, then $PR_{\text{Airy}} = 0.732$ mm and $PR_{\text{FWHM}} = 0.846$ mm, where $\lambda = c / f = 0.6$ mm. For the square of the Jinc function (i.e., intensity of the wave field or the two-way, i.e., transmit/receive response of an imaging system), the FWHM resolution (diffraction limit) is given by $PR_{\text{FWHM}}^2 = 2r_0 \approx 1.029 \lambda F / D = 0.6174$ mm since $\text{Jinc}^2(1.61633) = 0.5$ and thus $r_0 = 1.61633 F / (ka)$.

III. ULTRASOUND IMAGES FOR VISUAL (RETINA) STIMULATION OF THE BRAIN

Recently, it was found experimentally that when the retina of the eye is stimulated by ultrasound, corresponding neurons in particular positions of the brain produce electrical signals¹⁷. Thus, it is important to produce ultrasound images (beam patterns) from optical images captured by a digital camera in real time to assist blind people to “see” the surrounding objects. From Eq. (28), assuming that we would like a blind person to see an image (ultrasound beam pattern $\tilde{\Phi}(x_0, y_0, z = F; \omega)$) on the focal plane, an inverse Fourier transform

$\mathcal{G}_{k_{x_0}, k_{y_0}}^{-1}$ of the beam pattern with respect to k_{x_0} and k_{y_0} can be taken to find the modified driving function, $\tilde{\Phi}'_1(x_1, y_1; \omega)$ (this does not include the focusing phase shifts), on the surface of the transducer as follows:

$$\tilde{\Phi}'_1(x_1, y_1; \omega) = [i\lambda F e^{-ikF} (1 + \frac{i\lambda}{2\pi F})^{-1}] \int_{-\infty}^{\infty} \int_{-\infty}^{\infty} [\tilde{\Phi}(x_0, y_0, z = F; \omega) e^{-i\frac{k}{2F}(x_0^2 + y_0^2)}] e^{i(k_{x_0}x_1 + k_{y_0}y_1)} dk_{x_0} dk_{y_0}. \quad (38)$$

If the images are not formed on the $x_0 - y_0$ plane but on the spherical surface such as the retina, the phase term $\exp[-i\frac{k}{2F}(x_0^2 + y_0^2)] = \exp(-i\frac{k}{2F}r_0^2)$ in Eq. (38) should be removed when doing the inverse Fourier transform.

It is noticed that using the Bessel beams and X waves given in Eqs. (25) and (26), one also could design some ultrasound beam patterns that will stay in focus within their large depth of field²⁵. Or, using the zeroth-order Bessel beam ($n = 0$ in Eq. (25)), one could form ultrasound beam patterns by directly adding a shifted version of the beam. However, due to the high sidelobes of limited-diffraction beams, the image quality may be poor.

3. METHOD

A. HIGH-RESOLUTION IMAGING WITH FOCUSED J_0 BESSEL BEAM

In this study, an $f = 2.5$ -MHz frequency and $D = 50$ -mm diameter transducer was used. The transducer was electronically focused at $F = 50$ mm to produce a focused plane wave in transmit (see Eqs. (35) and (36)) and a focused zeroth-order Bessel beam $J_0(\alpha r_1)$ (see Eqs. (31) and (32)) in receive, where $\alpha = 1202.45 \text{ m}^{-1}$. As a comparison, the focused plane wave was used in both transmit and receive. C-mode images (image plane is perpendicular to the beam axis) of an object located at the focal plane of the beams were produced using these two different two-way (pulse-echo) imaging schemes²⁶.

B. ULTRASOUND IMAGES FOR VISUAL (RETINA) STIMULATION OF THE BRAIN

To produce an ultrasound image on the focal plane to perform visual (retina) stimulation of the brain¹⁷ to help certain blind people to “see” objects, the Verasonics 2D Matrix array transducer (7.5 MHz, 32x32 elements, 9.6 mm on each side, and a pitch of 0.3 mm or 1.5λ) and Eq. (38) was used.

4. RESULTS

The two-way (pulse-echo) beam profiles produced by a focused plane wave in transmit and a focused zeroth-order Bessel beam in receive, and by the focused plane wave in both transmit and receive are shown in Figs. 1(a) and 1(b), respectively. Figs. 2 and 3 are the two-way (pulse-echo) transverse beam profiles corresponding to Figs. 1(a) and 1(b) respectively at 9 different axial distances. Plots of transverse beam profiles through the beam center corresponding to those in Figs. 2 and 3 are given in Fig. 4. From these figures, it is clear that even though the Bessel beam is focused, it still has a larger depth of field and its sidelobes are suppressed by the focused plane wave. Fig. 5 shows an object consisting of 30 point scatterers used to get C-mode images (imaging plane is perpendicular to the beam axis). The C-mode image obtained by transverse scanning of the focused plane wave in transmit and the focused zeroth-order Bessel beam in receive is shown in Fig. 6(a). As a comparison, the image obtained with the focused plane wave in both transmit and receive is shown in Fig. 6(b). The parameters used to get Figs. 1-6 are in the legends of the corresponding figures or in the figures themselves. The image obtained with the focused Bessel beam in receive (Fig. 6(a)) has a higher two-way lateral resolution (0.56-mm FWHM) than that (0.66-mm FWHM) of image obtained using the focused plane wave in receive (Fig. 6(b)). The diffraction limit of the two-way lateral resolution of the focused plane wave in both transmit and receive calculated with the square of the Jinc function in Eq. (36)

is given by $PR_{FWHM}^2 \approx 1.029\lambda F/D = 0.62$ mm. Thus, using focused Bessel beam in receive, the lateral resolution exceeds the diffraction limit.

Figure 7 shows the results of ultrasound image (beam pattern) for visual (retina) stimulation of the brain according to Eq. (38). It is clear that such images can be produced with a commercial 2D array transducer with a relatively small number of elements (32x32 elements) and relatively large pitch (1.5λ). All the results in this paper were obtained using the method described in the 2005 paper¹⁰.

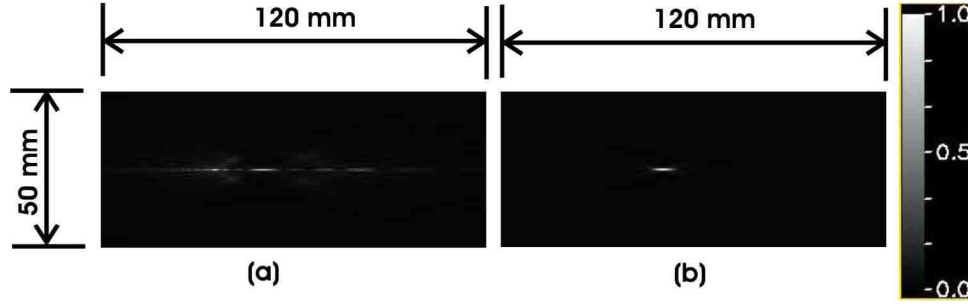


Figure 1. Axial two-way (pulse-echo) beam profile (normalized magnitude, see the grayscale bar) through the axis of the beam. A 2.5-MHz frequency and 50-mm diameter wave source was at the left edge of each image. The wavelength was 0.6 mm. (a) A focused plane wave was used in transmit and a focused $J_0(\alpha r_1)$ Bessel beam was used in receive ($\alpha = 1202.45 \text{ m}^{-1}$). (b) The focused plane wave was used in both transmit and receive.

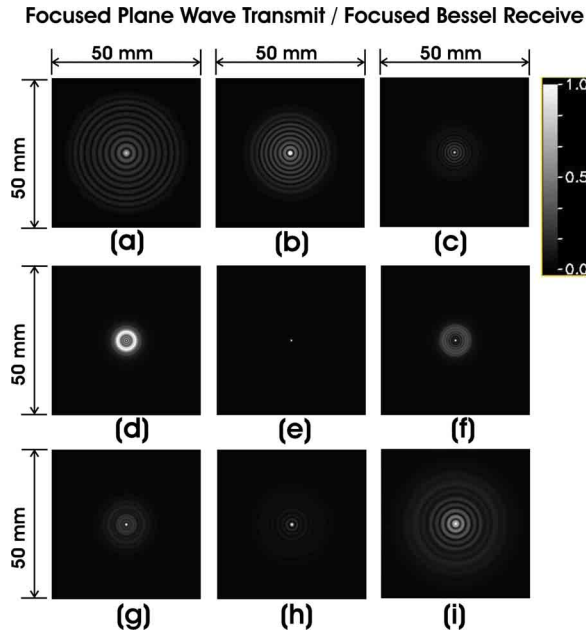


Figure 2. Transverse (perpendicular to the beam axis) two-way (pulse-echo) beam profiles (normalized magnitude) at axial distance of (a) 10, (b) 20, (c) 30, (d) 40, (e) 50 (focal distance), (f) 60, (g) 70, (h) 80, and (i) 90 mm, respectively. Focused plane wave was used in transmit and focused $J_0(\alpha r_1)$ Bessel beam was used in receive.

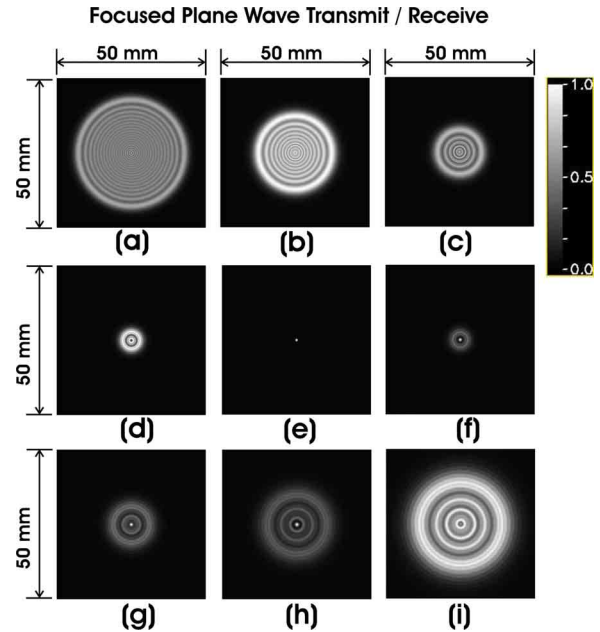


Figure 3. This figure is the same as Fig.2 except that the images were produced by using the focused plane wave in both transmit and receive.

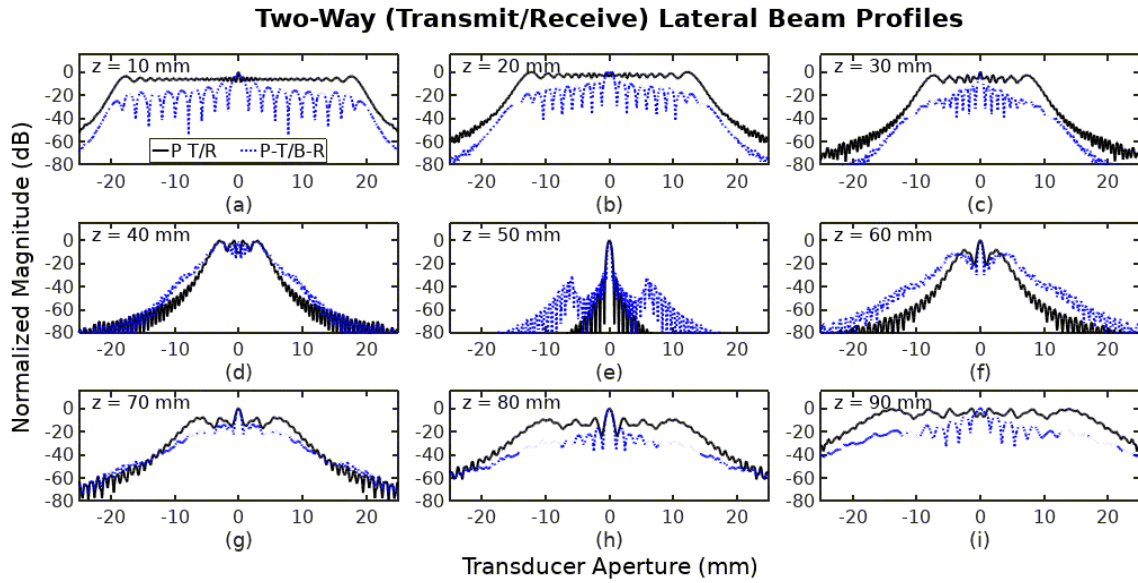


Figure 4. Transverse two-way (pulse-echo) beam plots across the center of the beam corresponding to images in Fig. 2 (blue dashed line) and Fig. 3 (black solid lines) respectively at 9 axial distances.

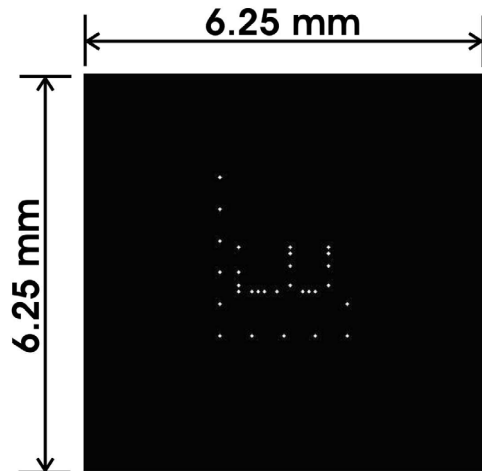


Figure 5. Object consisting of 30 point scatterers placed at the 50-mm focal plane of the transducer.

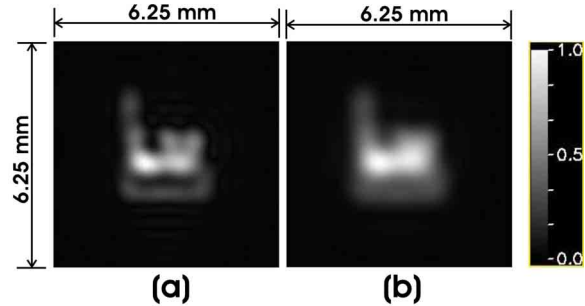


Figure 6. C-mode images produced by the two-way (pulse-echo) ultrasound beams in Figs. 1-4 and the point scatterers in Fig. 5. (a) Image produced by focused plane wave in transmit and focused $J_0(\alpha r_1)$ Bessel beam in receive. (b) Image produced by the focused plane wave in both transmit and receive.

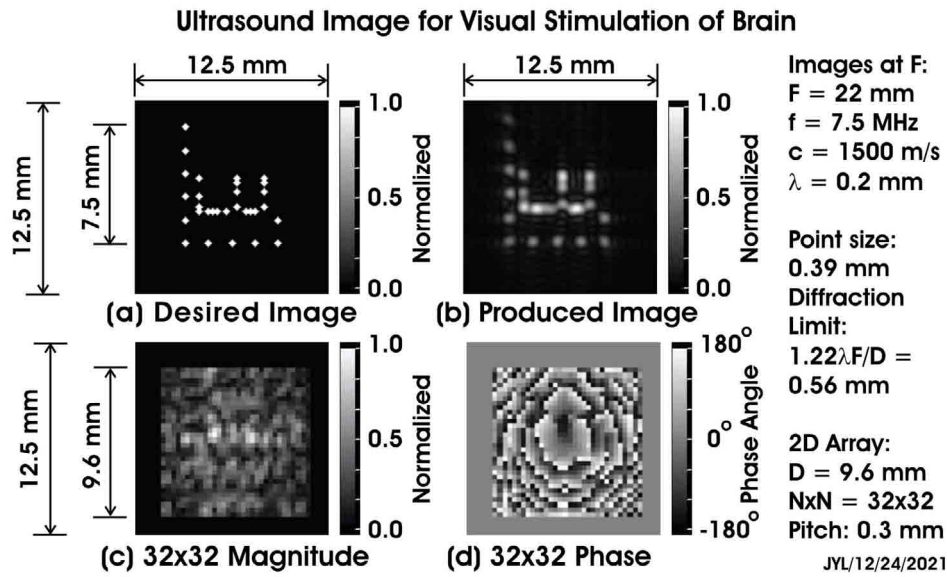


Figure 7. Ultrasound image (beam pattern) produced for visual (retina) stimulation of the brain. The parameters of the transducer and the object are shown in the figure. (a) Object consisting of 30 small points that a blind person wishes to see. (b) Ultrasound image produced at the retina to stimulate the brain of the blind person. (c) The normalized magnitude of the electrical signals to drive the elements of the ultrasound transducer to produce the image in (b). (d) The phases of the electrical signals to drive the transducer elements. The parameters of the transducer are the same as those of the Verasonics 2D Matrix array (<https://verasonics.com/matrix-array/>).

5. DISCUSSION AND CONCLUSION

In this paper, analytical solutions were obtained for various beams such as Bessel beams, X waves, and plane waves with and without focus in both rectangular and polar coordinates. Using a focused plane wave in transmit and a zeroth-order Bessel beam in receive, a C-mode image (imaging plane is perpendicular to the beam axis) at the focal distance was obtained. The lateral resolution of the image obtained was higher than the diffraction limit of the image obtained with the focused plane wave used in both transmit and receive. Although the Bessel beam was focused, it still has a larger depth of field than the conventional focused plane wave. The sidelobes of the Bessel beam were suppressed by the focused plane wave in transmit.

In addition, using the analytical solutions, an ultrasound image (beam pattern) that can be used for visual (retina) stimulation of the brain to help certain blind people to see objects was obtained.

ACKNOWLEDGMENTS

The author would like to thank Dr. Qifa Zhou and Mr. Gengxi Lu from the University of Southern California for discussions on the ultrasound visual stimulation of the brain.

REFERENCES

- ¹ J. Durnin. "Exact solutions for nondiffracting-beams. I. The scalar theory," *Journal of Optical Society of America*, vol. 4, no. 4, pp. 651-654, 1987.
- ² D. K. Hsu, F. I. Marccelan, and D. O. Thompson. "Bessel beam ultrasonic transducer: Fabrication method and experiment results," *Applied Physics Letter*, vol. 55, no. 2066, November, 1989.
- ³ Jian-yu Lu and J. F. Greenleaf, "Ultrasonic nondiffracting transducer for medical imaging," *IEEE Transactions on Ultrasonics, Ferroelectrics, and Frequency Control*, vol. 37, no. 5, pp. 438-447, September 1990.
- ⁴ Jian-yu Lu and J. F. Greenleaf, "Nondiffracting X waves --- exact solutions to free-space scalar wave equation and their finite aperture realizations," *IEEE Transactions on Ultrasonics, Ferroelectrics, and Frequency Control*, vol. 39, no. 1, pp. 19-31, January 1992.

- ⁵ Jian-yu Lu and J. F. Greenleaf, "Experimental verification of nondiffracting X waves," *IEEE Transactions on Ultrasonics, Ferroelectrics, and Frequency Control*, vol. 39, no. 3, pp. 441-446, May 1992.
- ⁶ Jian-yu Lu, Hehong Zou, and J. F. Greenleaf, "Biomedical ultrasound beam forming," *Ultrasound in Medicine and Biology*, vol. 20, no. 5, pp. 403-428, July 1994.
- ⁷ Jian-yu Lu, Zhaohui Wang, and Sung-Jae Kwon, "Blood flow velocity vector imaging with high frame rate imaging methods," in *2006 IEEE Ultrasonics Symposium Proceedings*, 06CH37777, vol. 2, pp. 963-966, 2006 (ISSN: 1051-0117).
- ⁸ Jian-yu Lu and J. F. Greenleaf, "Producing deep depth of field and depth-independent resolution in NDE with limited diffraction beams," *Ultrasonic Imaging*, vol. 15, no. 2, pp. 134-149, April 1993.
- ⁹ Jian-yu Lu and J. F. Greenleaf, "Evaluation of a nondiffracting transducer for tissue characterization," in *1990 IEEE Ultrasonics Symposium Proceedings*, 90CH2938-9, vol. 2, pp. 795-798, 1990 (ISSN: 1051-0117).
- ¹⁰ Jian-yu Lu and Jiqi Cheng, "Field computation for two-dimensional array transducers with limited diffraction array beams," *Ultrasonic Imaging*, vol. 27, no. 4, pp. 237-255, October 2005.
- ¹¹ Jian-yu Lu and Anjun Liu, "An X wave transform," *IEEE Transactions on Ultrasonics, Ferroelectrics, and Frequency Control*, vol. 47, no. 6, pp. 1472-1481, November 2000.
- ¹² Jian-yu Lu, "2D and 3D high frame rate imaging with limited diffraction beams," *IEEE Transactions on Ultrasonics, Ferroelectrics, and Frequency Control*, vol. 44, no. 4, pp. 839-856, July 1997.
- ¹³ Jian-yu Lu, "Experimental study of high frame rate imaging with limited diffraction beams," *IEEE Transactions on Ultrasonics, Ferroelectrics, and Frequency Control*, vol. 45, no. 1, pp. 84-97, January 1998.
- ¹⁴ Jian-yu Lu, Jiqi Cheng, and Jing Wang, "High frame rate imaging system for limited diffraction array beam imaging with square-wave aperture weightings," *IEEE Transactions on Ultrasonics, Ferroelectrics, and Frequency Control*, vol. 53, no. 10, pp. 1796-1812, October 2006.
- ¹⁵ Jiqi Cheng and Jian-yu Lu, "Extended high frame rate imaging method with limited diffraction beams," *IEEE Transactions on Ultrasonics, Ferroelectrics, and Frequency Control*, vol. 53, no. 5, pp. 880-899, May 2006.
- ¹⁶ James N. Steer, Alistair G. L. Borthwick, Miguel Onorato, Amin Chabchoub, and Ton S. van den Bremer, "Hydrodynamic X Waves," *Phys. Rev. Lett.* 123, 184501, October 29, 2019.
- ¹⁷ Gengxi Lu, Xuejun Qian, Runze Li, Bijou Thomas, Mark S. Humayun, and Qifa Zhou, "Non-invasive ultrasound stimulation on the retina and visual cortex for visual restoration," *Journal of Acoustical Society of America*, vol. 150, no. 4, pt. 2, pp. A207, 2021.
- ¹⁸ J. W. Goodman, *Introduction to Fourier Optics*. New York McGraw-Hill., 1968.
- ¹⁹ R. Bracewell. *The Fourier Transform and Its Applications*. New York: McGraw-Hill. 1965.
- ²⁰ P. M. Morse and H. Feshbach, *Methods of Theoretical Physics*. Part I, McGraw-Hill, New York, 1953.
- ²¹ Natalie Baddour, "Two-Dimensional Fourier Transforms in Polar Coordinates," *Advances in Imaging and Electron Physics*, Volume 165, ISSN 1076-5670, DOI: 10.1016/B978-0-12-385861-0.00001-4, 2011.
- ²² J. V. Cornacchio and R. P. Soni, "On a Relation Between Two-Dimensional Fourier Integrals and Series of Hankel Transforms," *Journal of Research of the National Bureau of Standards - B. Mathematics and Mathematical Physics*, Vol. 69B, No. 3, July-September 1965.
- ²³ M. S. Patterson and F. S. Foster, "Acoustic fields of conical radiators," *IEEE Transactions on Sonics and Ultrasonics*, vol. SU-29, no. 2, pp. 83-92, March 1982.
- ²⁴ I. S. Gradshteyn and I. M. Ryzhik, *Table of Integrals, Series, and Products*, 7th Edition, Academic Press, U.K., 2007.
- ²⁵ Jian-yu Lu, "Designing limited diffraction beams," *IEEE Transactions on Ultrasonics, Ferroelectrics, and Frequency Control*, vol. 44, no. 1, pp. 181-193, January 1997.
- ²⁶ Jian-yu Lu, "A Focused Limited-Diffraction Beam for High-Resolution Imaging," *Journal of Acoustical Society of America*, vol. 150 no. 4, pt. 2, pp. A88, 2021.